Three-dimensional Bose–Einstein condensate vortex solitons under optical lattice and harmonic confinements*

Wang Ying(王 莹), Zong Feng-De(宗丰德)†, and Li Feng-Bo(李峰波)

Institute of Nonlinear Physics, Zhejiang Normal University, Jinhua 321004, *China*

(Received 6 July 2012; revised manuscript received 6 September 2012)

We predict three-dimensional vortex solitons in a Bose–Einstein condensate under a complex potential, which is the combination of a two-dimensional parabolic trap along the transverse radial direction and a one-dimensional optical-lattice potential along the z axis direction. The vortex solitons are built in the form of a layer-chain structure made of several fundamental vortices along the optical-lattice direction. This has not been reported before in the three-dimensional Bose–Einstein condensate. By using a combination of the energy density functional method with direct numerical simulation, we find three-dimensional vortex solitons with topological charges $\chi = 1$, $\chi = 2$, and $\chi = 3$. Moreover, the macroscopic quantum tunneling and chirp phenomena of the vortex solitons are shown in the evolution. Therein, the occurrence of macroscopic quantum tunneling provides the possibility for the experimental realization of quantum tunneling. Specifically, we successfully manipulate the vortex solitons along the optical lattice direction. The stability limits for dragging the vortex solitons from an initial fixed position to a prescribed location are further pursued.

Keywords: Bose–Einstein condensates, Gross–Pitaevskii equation, vortex soliton, manipulation

PACS: 03.75.Lm, 03.75.Kk, 05.45.Yv **DOI:** 10.1088/1674-1056/22/3/030315

1. Introduction

In a one-dimensional (1D) trap, the localization and related topics of the Bose–Einstein condensate (BEC) have aroused numerous studies, both theoretically[1] and experimentally.[2,3] However, it has been challenging to investigate the dynamical patterns of three-dimensional matter-waves in the BEC. Although the creation of stable two-dimensional (2D) and three-dimensional (3D) solitons has become feasible in theory through numerous routes, the transient of BECs leads to the collapse of matter-waves in three-dimensional settings. It has been demonstrated that an optical lattice (OL) added to the Gross–Pitaevskii (GP) equation can successfully support BECs.[4] As we know, an OL is generated from the superposition of two counter-propagating laser beams with the same wavelength.[5] We also know that a BEC matter-wave can be stabilized by a quasi-1D[4] or quasi-2D[6,7] OL in the 2D or 3D space. However, only the 1D lattice trap cannot sustain a 3D matter-wave, except with an additional ingredient such as nonlinear management.[8] For this reason, BECs confined in a combined potential, which is made of an optical lattice and a harmonic trap, were discussed.[9–12] In situations with both attractive and repulsive nonlinearities, Nikolaos *et al*. systematically investigated the properties of lattice solitons,[9] and the evolution of a BEC soliton in an optical lattice and a harmonic trap was studied.[10] Recently, the dynamics of matter-wave solitons in harmonic traps with flashing optical lattices has also been studied analytically and numerically.[11] The motion of the solitary wave that is trapped in a potential consisting of linear magnetic and time-dependent laser fields is then manipulated by controlling the strengths of the fields.[12]

Here, we consider 3D BEC vortex solitons in a combined potential that consists of a 2D parabolic trap and a 1D OL confinement. Owing to the cylindrically symmetric structure and the oblate shape in the local external potential, we consider the linear superposition of several fundamental vortices. The vortex solitons are set to the layer-chain structures made up of several fundamental vortices along the OL direction. What is more, and distinct from the 3D harmonic traps in the other combined potentials (see Refs. [9] and [10]), the 2D parabolic trap is convenient for the manipulation of the 3D vortex solitons in the unconfined direction. For the BEC vortex solitons trapped in a harmonic confinement or in a 2D axially symmetric harmonic confinement, solitary vortices and the corresponding higher-order radial states were found in both the attractive and the repulsive nonlinearities.[13] And in the 3D parabolic trap, stable 3D spatially modulated vortex solitons were found in BECs.[14] For the BEC vortex solitons trapped in an OL, the OL restrains the splitting instability of the vortex solitons, even with a higher-order topological charge.[15,16] Yaroslav *et al*. found stable ring-profile vortex solitons, which are rare in nature.[16] Stable 2D vortices with a topological charge $\chi = 1$ were found in a cellular potential.[17] With the laser-induced lattice technique in photorefractive crystals, two-dimensional discrete vortices have

*Project supported by the National Natural Science Foundation of China (Grant Nos. 10672147 and 11072219) and the Natural Science Foundation of Zhejiang Province, China (Grant No. Y1080959).

†Corresponding author. E-mail: fdzong@zjnu.cn

© 2013 Chinese Physical Society and IOP Publishing Ltd

also been generated in photonic lattices.[18] Furthermore, it was found that three-dimensional novel classes of spatially localized vortex structures are supported in optical lattices.[19] What should also be mentioned is that the stable 3D vortex solitons were also made up of fundamental solitons and were built in the form of a rhombus consisting of four fundamental solitons in quasi-two-dimensional lattices.[7]

In this paper, we predict 3D BEC vortex solitons in the combined potential mentioned above, and realize the manipulation of the vortex solitons along the OL direction. It provides a way to establish stable matter-wave vortex solitons in the 3D space and paves a way for the control of 3D BECs. First, the existence and the dynamics of the 3D BEC vortex solitons are investigated via combining the energy density functional method[20–22] and the directly numerical simulation of the 3D GP equation. In order to prove the existence of the vortex solitons, we set the fundamental vortex at the valleys of the joint external potential. Since the BEC vortex solitons yield a local energy density minimum, the initial states of the stable solutions are searched by means of the energy density functional method. Then, we use the Crank–Nicholson discretization scheme[23,24] to directly simulate the time-dependent GP equation to test the stability of the vortex solitons. An important phenomenon is the chirp, i.e., the breathing oscillation of the vortex solitons over a long period of time, and the result further proves the stability of the vortex solitons. Meanwhile, the phenomenon of macroscopic quantum tunneling also arises. For macroscopic quantum tunneling, the reversal of the circulation of a vortex by quantum tunneling in a Bose gas trapped in a harmonic trap is investigated.[25] Cazalilla *et al.* studied the competition between vortex unbinding and tunneling in 2D Bose gases confined in a valley of a 1D optical lattice potential.[26] In a recent study, it was shown that a vortex can tunnel between two pinning potentials, providing the possibility to explore quantum tunneling experimentally,[27] as can the macroscopic quantum tunneling observed in the evolution of vortex solitons. Finally, we manipulate the stable vortex solitons successfully along the OL direction, and the stability limits are investigated.

This paper is organized as follows. In Section 2, we present a brief introduction of the nonlinear 3D time-dependent GP equation used in the paper, and adopt the energy density functional method to find the initial stable states. In Section 3, by using the Crank–Nicolson discretization scheme, we investigate some important phenomena in the evolution of vortex solitons. In Section 4, we manipulate the vortex solitons successfully along the z axis and find the areas to manipulate the vortex solitons. In addition, the factors that affect the possibility to manipulate the BECs are analyzed. In Section 5, we conclude the paper.

2. Model and energy density functional

The evolution of a BEC wave function can be described by the GP equation[28,29] at an extremely low temperature with a weak interaction. In the 3D case, the GP equation of a BEC matter-wave[30] is given in the following form:

$$\mathrm{i}\hbar\frac{\partial\Psi(\boldsymbol{r},t)}{\partial t}=\left[-\frac{\hbar^2}{2m}\nabla^2+g|\Psi(\boldsymbol{r},t)|^2+V(\boldsymbol{r})\right]\Psi(\boldsymbol{r},t), \quad (1)$$

where $\Psi(\boldsymbol{r},t)$ is the time-dependent BEC wave function, the nonlinear coefficient $g=4\pi a_s\hbar^2/m$ represents the interaction intensity between the BEC gases, m is the atomic mass, and a_s is the scattering length of the s-wave. The BEC is trapped in a combined external potential $V(\boldsymbol{r})$, consisting of an OL along the z axis and a harmonic confinement along the transverse radial direction. Additionally, the corresponding stationary solution $\Phi(\boldsymbol{r})$ is obtained by substituting $\Psi(\boldsymbol{r},t)=\Phi(\boldsymbol{r})\exp(-\mathrm{i}\mu t/\hbar)$ into Eq. (1). The corresponding energy density functional is

$$E(\Phi(\boldsymbol{r}))=\int \mathrm{d}^3r\left[\frac{\hbar^2}{2m}|\nabla\Phi(\boldsymbol{r})|^2+V(\boldsymbol{r})|\Phi(\boldsymbol{r})|^2+\frac{g}{2}|\Phi(\boldsymbol{r})|^4\right]. \quad (2)$$

The normalization condition is $\int \mathrm{d}^3r|\Psi(\boldsymbol{r},t)|^2=N$. Under the limit condition of almost zero temperature, N is the total atom number contained in the BEC.

In Eq. (1), we adopt the OL potential in the z direction as $V_{\mathrm{L}_\ell}(z)=V_0\cos^2(K(z-\bar{z}_\ell))$ ($\ell=1,2$. And when $\ell=1$, $\bar{z}_\ell=\bar{z}$; when $\ell=2$, $\bar{z}_\ell=\bar{z}+\pi/2K$). Hence, the external potential has the following form:

$$V_\ell(\boldsymbol{r})=\frac{m}{2}(x^2+y^2)+V_0\cos^2[K(z-\bar{z}_\ell)]. \quad (3)$$

Here, the OL strength is V_0 in units of recoil energy $E_0=2\pi^2\hbar^2/(m\lambda^2)$. The wave number and the wavelength of the OL are $K=2\pi/\lambda$ and λ, respectively, $\hbar$ is the reduced Planck constant. Moreover, $\rho=\sqrt{x^2+y^2}$ is the radial radius. The important parameter $\bar{z}$ is a function used to adjust the phase of the OL.

The axially symmetric trap makes it possible to create vortices in the BEC (see Ref. [31]). On these grounds, we consider a fundamental vortex that rotates around the z axis. As a result, the stationary BEC wave function $\Phi(\boldsymbol{r})$ can be expressed as

$$\Phi(\boldsymbol{r})=\psi(\boldsymbol{r})\exp(\mathrm{i}s), \quad (4)$$

where $|\psi(\boldsymbol{r})|^2$ is the atom number density of the BEC, phase $s=\chi\phi$ is the velocity potential, i.e., $\upsilon=(\hbar/m)\nabla s$, ϕ is the rotational angle around the z axis, and χ is the topological charge of the wave function. So the tangential velocity is $\upsilon_\perp=\hbar\chi/m\rho$. Since the GP equation was initially used to investigate the vortex in a Boson system with weak interaction, we replace the wave function $\Phi(\boldsymbol{r})$ in Eq. (2) with Eq. (4) and

introduce a centrifugal term. In addition, we take the dimensionless form in units of the radial resonance feature length $a_\perp = \sqrt{\hbar/m\omega_\perp}$ and the resonant characteristics energy $\hbar\omega_\perp$ ($\boldsymbol{r} \to \boldsymbol{r}/a_\perp$, $\varepsilon \to E(\Phi(\boldsymbol{r}))/(N\hbar\omega_\perp)$, the corresponding radial oscillator frequency is $\omega_\perp$). The corresponding wave function is $\psi(\boldsymbol{r}) \to \sqrt{a_\perp^3/N}\psi(\boldsymbol{r})$, which is normalized in the new coordinate system. The dimensionless parameter $\gamma = Na_s/a_\perp$ is important to characterize the interatomic interactions. Therefore, the GP energy density functionals of the BEC wave functions in external potentials $V_\ell(\boldsymbol{r})$ ($\ell = 1,2$) have the following form:

$$\varepsilon_\ell = \frac{1}{2}\int \mathrm{d}^3 r\{|\nabla\psi(\boldsymbol{r})|^2 + \{\chi^2\rho^{-2} + \rho^2 + V_0 \times \cos^2[K(z-\bar{z}_\ell)]\}|\psi(\boldsymbol{r})|^2 + 4\pi\gamma|\psi(\boldsymbol{r})|^4\}. \quad (5)$$

Expression $\frac{1}{2}\int \mathrm{d}^3 r\chi^2\rho^{-2}|\psi(\boldsymbol{r})|^2$ represents a centrifugal term and indicates the centrifuge field potential.

To find the stationary solutions of the vortex solitons, we try a fundamental vortex, which has been investigated (see Refs. [32] and [33]), in the following form:

$$\Phi_0(\boldsymbol{r}) = A\left(\frac{x+\mathrm{i}y}{k_\perp}\right)^\chi \exp\left[-\frac{1}{2}\left(\frac{\rho}{k_\perp}\right)^{\alpha_\perp} - \frac{1}{2}\left(\frac{z+z_1}{b_z}\right)^{\alpha_z}\right], \quad (6)$$

where parameter A is a normalization constant

$$A = \frac{\sqrt{\alpha_\perp\alpha_z}}{2k_\perp\sqrt{\pi b_z\Gamma[2(1+\chi)/\alpha_\perp]\Gamma(1/\alpha_z)}},$$

z_1 is a constant, and $\Gamma(\xi) = \int u^{\xi-1}\exp(-u)\,\mathrm{d}u$ ($\mathrm{Re}\,\xi > 0$) is the gamma function. Moreover, the density of the fundamental vortex generated in the transverse section is zero along the z axis. From the analysis above (cylindrically symmetric structure and oblate shape in the local of the external potential) and for the linear superposition, we adopt stationary two-vortex solitons (TWVSs) and stationary three-vortex solitons (TRVSs) in the following forms:

$$\Phi_2(\boldsymbol{r}) = \Phi_0(x,y,z+z_1) + \Phi_0(x,y,z-z_1), \quad (7)$$

$$\Phi_3(\boldsymbol{r}) = \Phi_0(x,y,z+z_1) + \Phi_0(x,y,z-z_1) + \Phi_0(x,y,z). \quad (8)$$

The normalization constants in the above systems are changed. The TWVSs are trapped in external potential $V_1(\boldsymbol{r})$, and the TRVSs are trapped in external potential $V_2(\boldsymbol{r})$. According to mathematical calculations, we study the energy density functionals of the vortex solitons. The energy density functionals of the stationary TWVSs and the stationary TRVSs are

$$\varepsilon_2 = \frac{\chi^2\Gamma(2\chi/\alpha_\perp)}{2k_\perp^2\Gamma[2(1+\chi)/\alpha_\perp]} - \frac{\chi\alpha_\perp\Gamma[(\alpha_\perp+2\chi)/\alpha_\perp]}{2k_\perp^2\Gamma[2(1+\chi)/\alpha_\perp]} + \frac{\alpha_\perp^2\Gamma[2(\alpha_\perp+\chi)/\alpha_\perp]}{8k_\perp^2\Gamma[2(1+\chi)/\alpha_\perp]} + \frac{1}{4}V_0 + \frac{k_\perp^2\Gamma[2(2+\chi)/\alpha_\perp]}{2\Gamma[2(1+\chi)/\alpha_\perp]}$$
$$- \frac{z_1^2\exp\left[-\left(\frac{z_1}{b_z}\right)^2\right]}{b_z^4\left(1+\exp\left[-\left(\frac{z_1}{b_z}\right)^2\right]\right)} - \frac{1}{4}\exp[-(b_z^2k^2)]$$
$$\times \frac{V_0}{1+\exp\left[-\left(\frac{z_1}{b_z}\right)^2\right]}\left\{\frac{\cos[2K(\bar{z}+z_1)]}{2} + \frac{\cos[2K(\bar{z}-z_1)]}{2} + \exp\left[-\left(\frac{z_1}{b_z}\right)^2\right]\cos(2K\bar{z})\right\}$$
$$+ \frac{1}{4}\frac{1}{\left(1+\exp\left[-\left(\frac{z_1}{b_z}\right)^2\right]\right)^2} \times \left\{2+6\exp\left[-2\left(\frac{z_1}{b_z}\right)^2\right] + 8\exp\left[-\frac{3}{2}\left(\frac{z_1}{b_z}\right)^2\right]\right\}$$
$$\times 2^{-1-\frac{4\chi+2}{\alpha_\perp}-\frac{1}{\alpha_z}}\frac{\gamma\alpha_\perp\alpha_z}{k_\perp^2 b_z}\frac{\Gamma[2(1+2\chi)/\alpha_\perp]}{\Gamma[2(1+\chi)/\alpha_\perp]^2\Gamma(1/\alpha_z)} + \frac{\alpha_z^2\Gamma\left(2-\frac{1}{\alpha_z}\right)}{8b_z^2\Gamma(1/\alpha_z)}, \quad (9)$$

$$\varepsilon_3 = \frac{\chi^2\Gamma(2\chi/\alpha_\perp)}{2k_\perp^2\Gamma[2(1+\chi)/\alpha_\perp]} - \frac{\chi\alpha_\perp\Gamma[(\alpha_\perp+2\chi)/\alpha_\perp]}{2k_\perp^2\Gamma[2(1+\chi)/\alpha_\perp]} + \frac{\alpha_\perp^2\Gamma[2(\alpha_\perp+\chi)/\alpha_\perp]}{8k_\perp^2\Gamma[2(1+\chi)/\alpha_\perp]} + \frac{1}{4}V_0 + \frac{\alpha_z^2\Gamma(2-\frac{1}{\alpha_z})}{8b_z^2\Gamma(1/\alpha_z)}$$
$$- \frac{z_1^2\exp\left[-\left(\frac{z_1}{b_z}\right)^2\right]}{b_z^4\left(3+2\exp\left[-\left(\frac{z_1}{b_z}\right)^2\right]+4\exp\left[-\left(\frac{z_1}{2b_z}\right)^2\right]\right)} + \frac{k_\perp^2\Gamma[2(2+\chi)/\alpha_\perp]}{2\Gamma[2(1+\chi)/\alpha_\perp]}$$
$$- \frac{z_1^2\exp\left[-\left(\frac{z_1}{2b_z}\right)^2\right]}{2b_z^4\left(3+2\exp\left[-\left(\frac{z_1}{b_z}\right)^2\right]+4\exp\left[-\left(\frac{z_1}{2b_z}\right)^2\right]\right)} - \frac{1}{4}\frac{V_0}{3+2\exp\left[-\left(\frac{z_1}{b_z}\right)^2\right]+4\exp\left[-\left(\frac{z_1}{2b_z}\right)^2\right]}$$
$$\times \left\{\cos(2K\bar{z}) + 2\cos(2K\bar{z})\exp\left[-\left(\frac{z_1}{b_z}\right)^2\right] + \cos[2K(\bar{z}+z_1)] + \cos[2K(\bar{z}-z_1)] + 2\exp\left[-\left(\frac{z_1}{2b_z}\right)^2\right] \times \left(\cos\left[2K\left(\bar{z}+\frac{z_1}{2}\right)\right] + \cos\left[2K\left(\bar{z}-\frac{z_1}{2}\right)\right]\right)\right\}$$
$$\times \exp[-(b_z^2k^2)] + 2^{-1-\frac{4\chi+2}{\alpha_\perp}-\frac{1}{\alpha_z}} \times \frac{1}{\left(3+2\exp\left[-\left(\frac{z_1}{b_z}\right)^2\right]+4\exp\left[-\left(\frac{z_1}{2b_z}\right)^2\right]\right)^2}$$

$$\times\left\{3+6\exp\left[-2\left(\frac{z_1}{b_z}\right)^2\right]+8\exp\left[-\frac{3}{2}\left(\frac{z_1}{b_z}\right)^2\right]\right.$$
$$+12\exp\left[-\left(\frac{z_1}{b_z}\right)^2\right]+12\exp\left[-2\left(\frac{z_1}{2b_z}\right)^2\right]$$
$$\left.+16\exp\left[-\frac{3}{8}\left(\frac{z_1}{b_z}\right)^2\right]+24\exp\left[-\frac{11}{8}\left(\frac{z_1}{b_z}\right)^2\right]\right\}$$
$$\times\frac{\gamma\alpha_\perp\alpha_z\Gamma[2(1+2\chi)/\alpha_\perp]}{k_\perp^2 b_z\Gamma[2(1+\chi)/\alpha_\perp]^2\Gamma(1/\alpha_z)}. \quad (10)$$

The above energy density functionals are polynomial functions of undetermined dimensionless parameters $\alpha_\perp$, α_z, $k_\perp$, and b_z. $\alpha_\perp$ features the resonance characteristic length, in a radial scale, of vortex soliton atoms, α_z features the resonance characteristic length, in an axial scale, of vortex soliton atoms, and $k_\perp$ and b_z indicate the changes in radial and axial scales of vortex soliton atoms caused by the interatomic interactions, respectively. The scopes of the variable quantities are discussed in the next section. By analogy, the energy density functionals of vortex solitons ε_n $(n \geq 4)$ can also be obtained. The particle swarm optimization (PSO) algorithm can be applied to solve the extremum problem of a multivariate function. Hence we obtain the locally optimal solutions of the trial functions by using the PSO to search the minima of the energy density functionals. For the PSO technique, a theoretical overview of it has been presented.[34] Naturally, the PSO technique has been used in some physical applications, such as in predicting a crystal structure[35] and the parameter extraction of silicon solar cells.[36]

3. Dynamic characteristics of vortex solitons

In order to find stable vortex solitons, the undetermined parameters in the energy density functionals above are subject to $\alpha_\perp = 2$, $\alpha_z = 2$, $0 < k_\perp \leq 2.5$, and $0 < b_z \leq 1.2$. The sets are acquired through a large number of numerical calculations with the help of the PSO technique. Firstly, the initial states of the vortex solitons are searched using the PSO technique. Next, the Crank–Nicholson discretization scheme is employed to examine the stability of the vortex solitons. The precision of the Crank–Nicholson discretization scheme is confirmed by regulating the space and time steps. The space and time steps employed here are 0.075 and 0.001, respectively. The parameters (the radial resonance feature length $a_\perp = 1.222\times10^{-4}$ and the scattering to resonance length ratio $a_s/a_\perp = 4.33\times10^{-3}$) in this paper are taken from Ref. [37]. The nonlinear coefficient $g = 4\pi a_s\hbar^2/m > 0$ indicates that the nonlinear interactions in the GP equations below are self-repulsive. To our knowledge, a Bose–Einstein condensate with repulsive interaction was observed in a vapor of rubidium-87 atoms.[38] In this part, we firstly consider the TWVSs. The wave functions adopt the form presented in Eq. (7). The vortex solitons are trapped in an external potential consisting of an OL and a harmonic confinement, as shown in Fig. 1. In the figure, the OL strength is 50, and the wave number of the OL is 1. As shown from the isosurface and the slice plot of the trap, we know that the structure of the external potential is cylindrically symmetric. The fundamental vortex soliton can be trapped in the external potential firmly because it is just like a harmonic confinement in the local areas. It also offers a great chance to create 3D vortex solitons experimentally.

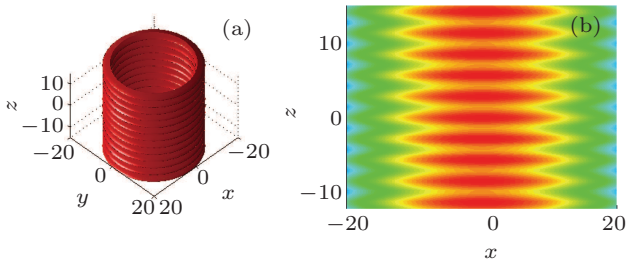


Fig. 1. (color online) (a) The three-dimensional isosurface of the trap. The corresponding OL is $V_{L1}(z) = V_0\cos^2[K(z-\bar{z})]$, whose value is 150. (b) Slice plot of the external potential in the midplane $y = 0$.

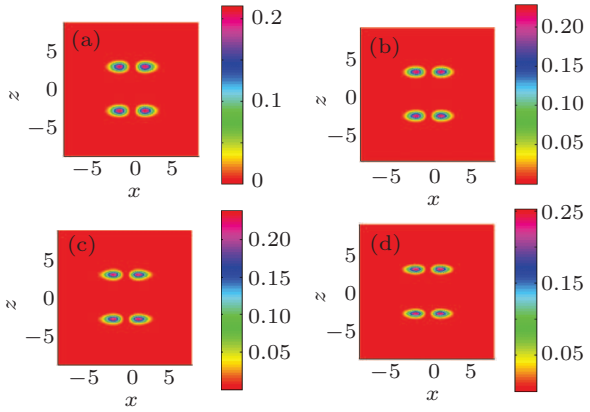


Fig. 2. (color online) Slice plots of a two-vortex soliton in the midplane $y = 0$ at different times ((a) $t = 0$, (b) $t = 40$, (c) $t = 60$, (d) $t = 80$). The parameters of the two-vortex soliton with a topological charge $\chi = 3$ are $N = 500$, $\alpha_\perp = 2$, $\alpha_z = 2$, $k_\perp = 1.0397$, and $b_z = 0.4009$. The wave number of the OL is $K = 1$, and the OL strength V_0 is 50.

As shown in Fig. 2, we obtain a stable TWVS under the confinement with topological charge $\chi = 3$. First, we symmetrically distribute the two fundamental vortices of the TWVS on both sides of the z axis. The corresponding position of the upper fundamental vortex is $z_1 = \pi/K = \pi$. A stable initial state is achieved by applying the energy density functional method. For the stable initial state, the proper parameters are searched for by modulating the radial scale alteration $k_\perp$ and the axial scale alteration b_z of the TWVS on the basis of the Gauss anstaz. When the energy density functional of the TWVS approaches the minimum, the BEC becomes stable under the influence of the interatomic interaction, the impact between the fundamental vortices, the gravity of the TWVS atoms, and the external potential. Next, we perform a direct numerical simulation of its evolution by using the Crank–Nicholson discretization scheme in a grid of $256\times256\times256$ over the boundary from -9.6 to 9.525. From the slice plots at

different times, we know that the TWVSs are approximately unchanged in the evolution. The corresponding phase plots are shown in Fig. 3. The total evolving duration $t = 80$ is a dimensionless constant, which is long enough to demonstrate the stability of the BEC. Using the same process, we also get stable TWVSs with $\chi = 1$ and $\chi = 2$. Thus, the results shown here present the existence of TWVSs with $\chi = 1$, $\chi = 2$, and $\chi = 3$.

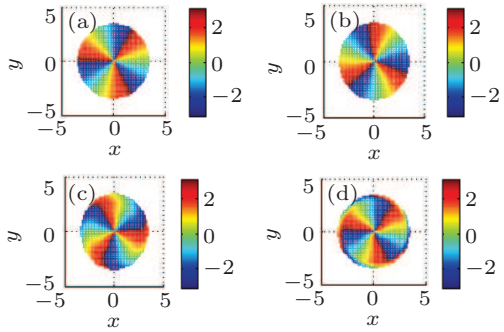


Fig. 3. (color online) The corresponding phase evolution plots for the two-vortex soliton shown in Fig. 2 ((a) $t = 0$, (b) $t = 40$, (c) $t = 60$, (d) $t = 80$).

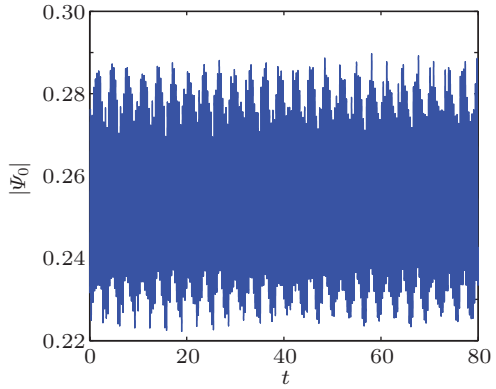


Fig. 4. (color online) Amplitude evolution plot of a fundamental vortex $|\Psi_0(\boldsymbol{r},t)|$ in a two-vortex soliton obtained by direct numerical simulation with topological charge $\chi = 3$. The parameters are the same as those in Fig. 2. The amplitude evolution is over time $t = 80$.

The amplitude variation of a fundamental vortex of the TWVS with $\chi = 3$ is shown in Fig. 4. The fairly stable periodic variation further demonstrates the stability of the TWVS with an appropriate parameter setting. In the figure, we observe the double cyclical phenomenon. We discover that the periods of the TWVS are $T_1 = 3.3$ (the major cycle) and $T_2 = 0.35$ (the minor cycle embedded in the major cycle). The major cycle is generated by the local parabolical trap, and the minor cycle is generated by the periodicity of the OL. Moreover, we observe that the pulse width of the TWVS transforms in the period from Fig. 5. In fact, we find that the amplitude and the pulse width of the TWVS change together. As a result, the behavior of the TWVS is space localized and periodic in time, i.e., the breathing vortex solitons. The product of amplitudes and pulse widths in the radial direction at different times is an approximately unchanged value, which is the chirp phenomenon.[37,38] The chirp of a 2D dispersion-managed soliton was successfully obtained and could be used to describe the long time evolution of the soliton.[39] In addition, the dynamics of the breathing and the quasibreathing solitons were discussed in two-component Bose–Einstein condensates with time- and space-modulated nonlinearities.[40] Here, the chirp phenomenon of the TWVS observed in the long-time evolution also presents the dynamics of the breathing TWVS. It is worth noting that the chirp causes quadratic phase changes and then leads to the variations in the phase evolution plots in Figs. 3 and 8.

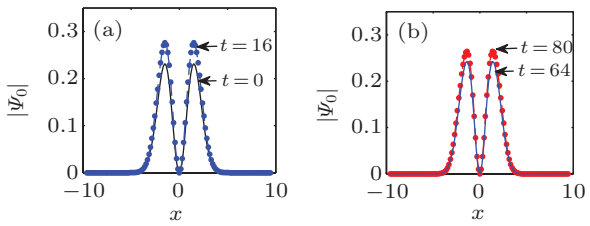


Fig. 5. (color online) Amplitude and pulse width distributions of the two-vortex soliton at (a) $t = 0$, $t = 16$ and (b) at $t = 64$, $t = 80$. The parameters are the same as those in Fig. 2.

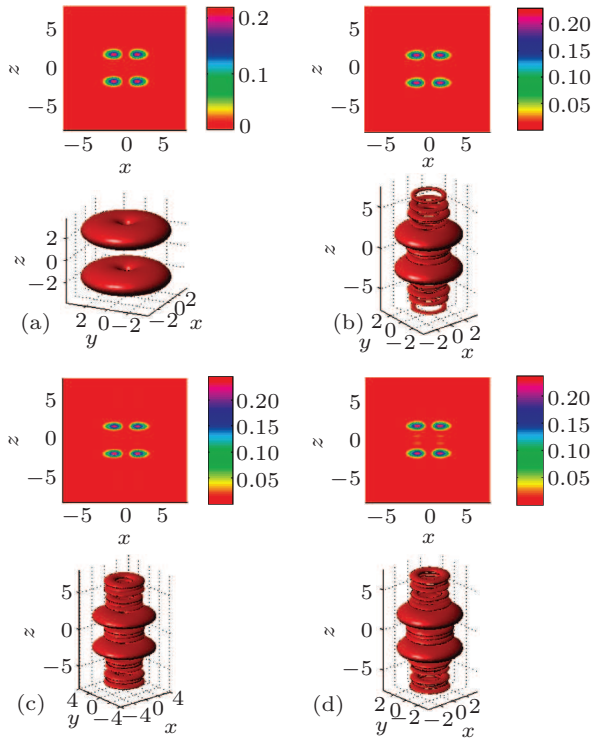


Fig. 6. (color online) The tunneling phenomenon of a two-vortex soliton with topological charge $\chi = 3$ for $N = 500$, $\alpha_\perp = 2$, $\alpha_z = 2$, $\kappa_\perp = 1.0408$, and $b_z = 0.3887$. The wave number of the OL is $K = 1.5$, and the OL strength V_0 is 30. (a) The initial state of the tunneling process. The upper figure is the slice plot in the midplane $y = 0$ of the two-vortex soliton, and the lower figure is the amplitude isosurface for the value of 0.01. Panels (b), (c), and (d) are the plots for $t = 40$, $t = 60$, and $t = 80$, respectively.

Another important phenomenon is the appearance of macroscopic quantum tunneling.[25–27,41] As presented in Fig. 6, the lifetime of the TWVS reduces when the quantum depletion of the TWVS turns up. And this occurs at the time when the atoms tunnel into another notch. It is worth

mentioning that the depletion of Bose gases has been investigated in optical lattices of nearest neighbors characterized by pair tunneling within mean-field theory.[42] The two kinds of tunneling both occur between nearest-neighbor matter-waves. Next, we discuss the conditions for the appearance of macroscopic quantum tunneling. This is prone to occur when the OL strength is not strong enough to trap the TWVS tightly. Because of the OL along the z axis direction, the lattice potential should be deep enough to make the TWVS hold against the gravity of the TWVS atoms. We also know that the tunneling phenomenon is caused by the co-action of the TWVS interatomic interaction, the impact between fundamental vortices of the vortex soliton, the gravity of the TWVS atoms, and the external potential. Because the gravity of the TWVS atoms is tiny, the circumstances of the TWVS are similar to the microgravity environment. Thus, we may be able to measure microgravity by measuring the macroscopic quantum tunneling of the TWVS.

After discussing the existence and the dynamics of the TWVS, we can also testify the stabilities of TRVSs with topological charges $\chi = 1$, $\chi = 2$, and $\chi = 3$. A stable TRVS with a topological charge $\chi = 3$ is shown in Fig. 7, and the corresponding phase plots are shown in Fig. 8.

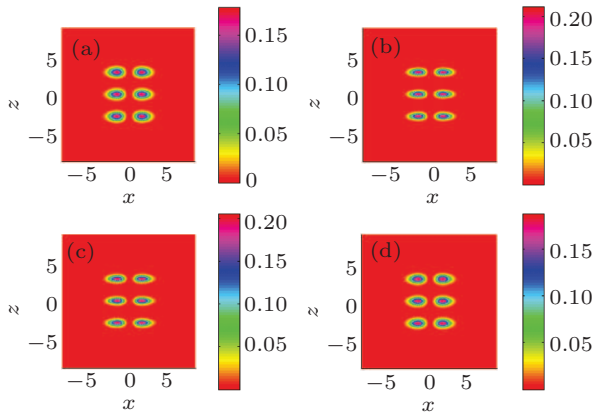


Fig. 7. (color online) Slice plots of a three-vortex soliton in the midplane $y = 0$ at different times ((a) $t = 0$, (b) $t = 40$, (c) $t = 60$, (d) $t = 80$). The parameters of the three-vortex soliton with topological charge $\chi = 3$ are $N = 500$, $\alpha_\perp = 2$, $\alpha_z = 2$, $k_\perp = 1.0272$, and $b_z = 0.3977$. The wave number of the OL is $K = 1$, and the OL strength V_0 is 50.

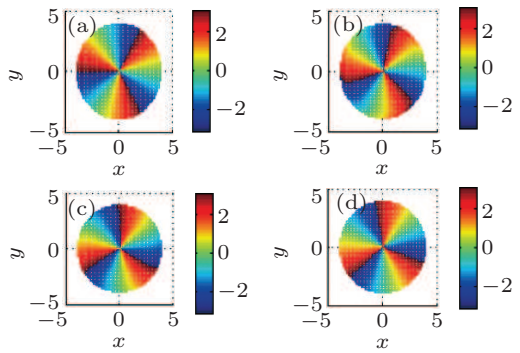


Fig. 8. (color online) The corresponding phase evolution plots for the three-vortex soliton shown in Fig. 7 ((a) $t = 0$, (b) $t = 40$, (c) $t = 60$, (d) $t = 80$).

4. Manipulation of vortex solitons

Now we concentrate on the manipulation of TRVSs. The methods used to manipulate dark solitons by switching the OL on adiabatically or moving the OL slowly[43] have been discussed in detail. In addition, controlling the motion of bright matter-wave solitons by means of periodic potentials[44] has been realized successfully. Here, we drag an initially stable TRVS to a specified destination by moving the OL tardily. There is only a $\pi/2$ phase difference between the external potentials $V_2(\boldsymbol{r})$ and $V_1(\boldsymbol{r})$ shown in Fig. 1. From Fig. 1, we notice that the structure of the trap potential $V_2(\boldsymbol{r})$ is cylindrically symmetric, and the OL set in the z axis can be shifted randomly along the z axis direction, but the construction of the confinement remains unchanged. Consequently, this provides the possibility to realize the manipulation of the vortex solitons along the z axis direction.

This is experimentally feasible because the phase of the OL can be tuned by modulating the angle between the counter-propagating laser beams, which can be realized by using acousto-optic modulators.[45] We must ensure that the velocity of the motion is slow enough to ensure the stability of the TRVS. Otherwise, the original vortex solitons ultimately escape because of the continuous dissipation of energy. Owing to the concept of the prescribed movement of solitons in the lattice,[46] we choose the control function $\bar{z}(t)$ in the external potential (Eq. (3)) as follows:

$$\bar{z}(t) = z_{\rm i} + (1/2)(z_{\rm f} - z_{\rm i})\{1 + \tanh[(t - t_0)/\tau]\}, \qquad (11)$$

where $z_{\rm i}$ is the initial position, and $z_{\rm f}$ is the destination. τ displays the dragging time length, and t_0 presents the beginning of the shift. The maximal velocity $\upsilon_{\max} = |z_{\rm f} - z_{\rm i}|/(2\tau)$ must be small enough to make the process adiabatical. The control function plays a significant role in the manipulation.

As shown in Fig. 9, we move the medially fundamental vortex of the TRVS with $\chi = 3$ successfully from $z_i = 0$ to $z_{\rm f} = \pi/K$. Figure 9(e) presents the evolution of the manipulation by the amplitude isosurface distribution with a value of 0.1. By steadily moving the OL, the vortex soliton is dragged to the specified point in a prescribed path. The slope in the panel reflects the traveling speed, namely, the greater the gradient of the isosurface, the faster the shifting of the OL. The period fluctuation with a small amplitude is also found in the dragging process. This is because the initial vortex soliton is not completely located at the valleys of the external potential.

The manipulation of the TRVS with $\chi = 1$ or $\chi = 2$ is also achieved in the same way. We also get the stability regions to manipulate them successfully by performing a large amount of numerical simulations with a certain range of τ. Naturally, we find the critical boundary of τ from 0.3 to 50. When the moving speed is too fast or too slow, the vortex solitons will oscillate drastically and collapse. We show the regions in

which the TRVSs can be manipulated successfully in Fig. 10. The values on the curves are the critical conditions, and the regions above them are the ones demanded in manipulating the TRVSs. From the figure, we can conclude that the manipulation of the TRVS is also related to the depth and the wave number of the OL. For the critical values of the successful manipulation, the results can be divided into three segments. When the wave number of the OL is between $K = 0.3$ and $K = 0.7$, the strength of the OL decreases with the increase in the wave number with topological charge $\chi = 1$ and $\chi = 3$. But the strength of the OL increases with the increase in the wave number with topological charge $\chi = 2$. Among them, the TRVS with topological charge $\chi = 3$ requires the strongest confinement, and the TRVS with topological charge $\chi = 2$ needs the weakest confinement under the same wave number. When the wave number of the OL is between $K = 0.7$ and $K = 1.7$, the strength of the OL increases with the increase in the wave number. The topological charge of the TRVS has little effect on its stability. When the wave number of the OL is between $K = 1.7$ and $K = 1.9$, the strength of the OL decreases with the increase in the wave number with topological charge $\chi = 1$ and $\chi = 3$. But the strength of the OL increases with the increase in the wave number with topological charge $\chi = 2$. Among them, the TRVS with topological charge $\chi = 2$ requires the strongest confinement and the TRVS with topological charge $\chi = 3$ needs the weakest confinement under the same wave number. In the case of a weak OL strength, the TRVS cannot be trapped. So we can remove a TRVS successfully by increasing the OL strength.

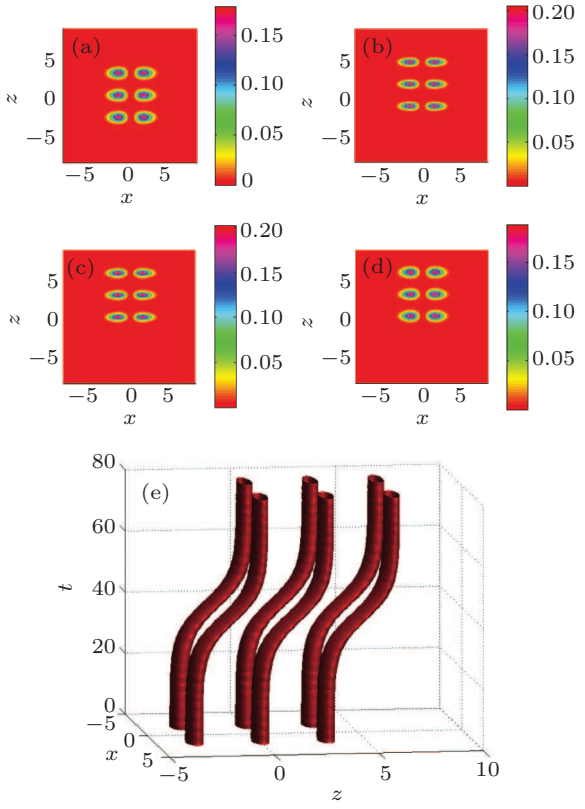


Fig. 9. (color online) The successful manipulation of a three-vortex soliton with topological charge $\chi = 3$ dragged along the z axis for $N = 500$, $\alpha_\perp = 2$, $\alpha_z = 2$, $k_\perp = 1.0357$, and $b_z = 0.2931$. The wave number of the OL is $K = 1$, the OL strength V_0 is 90, and the value of τ is 10. Panels (a), (b), (c), and (d) show the slice plots in the midplane $y = 0$ at $t = 0$, $t = 40$, $t = 60$, and $t = 80$, respectively. (e) Targeted shift of the three-vortex soliton from $z_i = 0$ to $z_f = \pi/K$, represented by the evolution of isosurface distribution. The value of the amplitude isosurface is 0.1.

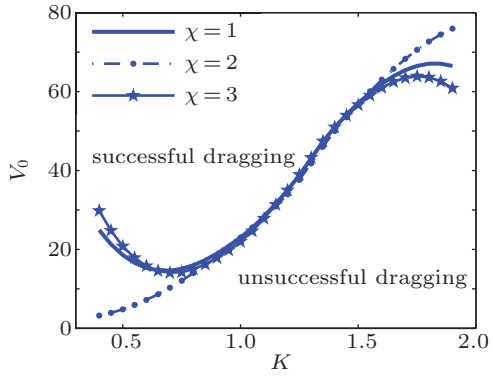


Fig. 10. (color online) Curves representing the critical values for manipulating three-vortex solitons with topological charges $\chi = 1$, $\chi = 2$, and $\chi = 3$. The areas above these curves are the stable regions to manipulate the three-vortex solitons.

5. Conclusion

We set up stable 3D BEC vortex solitons, in the form of a layer-chain structure made up of several fundamental vortices, by combining the energy density functional method and direct numerical simulation. We studied the stability, dynamics, and manipulation of the 3D BEC vortex solitons trapped in a complex potential consisting of an OL potential along the z axis direction and a parabolic potential along the transverse radial direction. The stable 3D vortex solitons are diverse, with topological charges $\chi = 1$, $\chi = 2$, and $\chi = 3$. First, we apply the PSO to optimize the energy density functional to find the stable initial states of the vortex solitons. Subsequently, the stability of the solutions is verified by direct numerical simulations. In addition, the phenomena of chirp and tunneling are also observed in the process. Finally, the drag of the vortex solitons along the OL direction is realized, and we analyze the influence factors that impede the removal of the vortex solitons and find the limit areas. However, due to PC limitations we only investigated the results for TWVSs and TRVSs. We hope that this study could stimulate the realization of 3D BECs owing to the experimental feasibility of the external potential here. Besides, the successful manipulation of vortex solitons can be adapted in quantum information storage and processing because the BEC can be used as a carrier of information.

References

[1] Morsch O and Oberthaler M 2006 *Rev. Mod. Phys.* **78** 179
[2] Billy J, Josse V, Zuo Z, Bernard A, Hambrecht B, Lugan P, Clment D, Sanchez P L, Bouyer P and Aspect A 2008 *Nature* **453** 891

[3] Roati G, D'Errico C, Fallani L, Fattori M, Fort C, Zaccanti M, Modugno G, Modugno M and Inguscio M 2008 *Nature* **453** 895

[4] Baizakov B B, Malomed B A and Salerno M 2004 *Phys. Rev. A* **70** 053614

[5] Cataliotti F S, Burger S, Fort C, Maddaloni P, Minardi F, Trombettoni A, Smerzi A and Inguscio M 2001 *Science* **293** 843

[6] Mihalache D, Mazilu D, Lederer F, Kartashov Y V, Crasovan L C and Torner L 2004 *Phys. Rev. E* **70** 055603

[7] Leblond H, Malomed B A and Mihalache D 2007 *Phys. Rev. E* **76** 026604

[8] Matuszewski M, Infeld E, Malomed B A and Trippenbach M 2005 *Phys. Rev. Lett.* **95** 050403

[9] Efremidis N K and Christodoulides D N 2003 *Phys. Rev. A* **67** 063608

[10] Zhang R, Sapiro R E, Mhaskar R R and Raithel G 2008 *Phys. Rev. A* **78** 053607

[11] Alexander T J, Heenan K, Salerno M and Ostrovskaya E A 2012 *Phys. Rev. A* **85** 063626

[12] Etienne W, Timoléon C K and Alidou M 2012 *Chin. Phys. B* **21** 070504

[13] Wu L, Li L, Zhang J F, Mihalache D, Malomed Boris A and Liu W M 2010 *Phys. Rev. A* **81** 061805

[14] Volodymyr L M 2008 *Phys. Rev. A* **78** 033603

[15] Sakaguchi H and Malomed B A 2005 *Europhys. Lett.* **72** 698

[16] Kartashov Y V, Vysloukh V A and Torner L 2005 *Phys. Rev. Lett.* **94** 043902

[17] Baizakov B B, Malomed B A and Salerno M 2003 *Europhys. Lett.* **63** 642

[18] Neshev D N, Alexander T J, Ostrovskaya E A, Kivshar Y S, Martin H, Makasyuk I and Chen Z 2004 *Phys. Rev. Lett.* **92** 123903

[19] Tristram J A, Elena A O, Andrey A S and Yuri S K 2005 *Phys. Rev. A* **72** 043603

[20] Hu J H, Wang J J, Gao X L, Okumura M, Igarashi R, Yamada S and Machida M 2010 *Phys. Rev. B* **82** 014202

[21] Gao X l, Polini M, Tosi M P, Vivaldo L, Campo J, Capelle K and Rigol M 2006 *Phys. Rev. B* **73** 165120

[22] Baym G and Pethick C J 2004 *Phys. Rev. A* **69** 043619

[23] Muruganandam P and Adhikari S K 2009 *Comput. Phys. Commun.* **180** 1888

[24] Muruganandam P and Adhikari S K 2003 *J. Phys. B: At. Mol. Opt. Phys.* **36** 2501

[25] Watanabe G and Pethick C J 2007 *Phys. Rev. A* **76** 021605

[26] Cazalilla M A, Iucci A and Giamarchi T 2007 *Phys. Rev. A* **75** 051603

[27] Fialko O, Bradley A S and Brand J 2012 *Phys. Rev. Lett.* **108** 015301

[28] Gross E P 1963 *J. Math. Phys.* **4** 195

[29] Gross E P 1961 *Nuovo Cimento* **20** 454

[30] Dalfovo F, Giorgini S, Pitaevskii L P and Stringari S 1999 *Rev. Mod. Phys.* **71** 463

[31] Adhikari S K 2010 *Phys. Rev. A* **81** 043636

[32] Xu Z J, Shi J Q and Lin G C 2007 *Acta Phys. Sin.* **56** 0666 (in Chinese)

[33] Tikhonenkov I, Malomed B A and Vardi A 2008 *Phys. Rev. A* **78** 043614

[34] Robinson J and Rahmat-Samii Y 2004 *IEEE Transactions on Antennas and Propagation* **52** 397

[35] Wang Y, Lv J, Zhu L and Ma Y 2010 *Phys. Rev. B* **82** 094116

[36] Ye M, Wang X and Xu Y 2009 *J. Appl. Phys.* **105** 094502

[37] Dalfovo F and Stringari S 1996 *Phys. Rev. A* **53** 2477

[38] Anderson M H, Ensher J R, Matthews M R, Wieman C E and Cornell E A 1995 *Science* **269** 198

[39] Abdullaev F K, Baizakov B B and Salerno M 2003 *Phys. Rev. E* **68** 066605

[40] Wang D S, Hu X H and Liu W M 2010 *Phys. Rev. A* **82** 023612

[41] Anderson B P and Kasevich M A 1998 *Science* **282** 1686

[42] Wang Y M and Liang J Q 2012 *Chin. Phys. B* **21** 060305

[43] Theocharis G, Frantzeskakis D J, Carretero-González R, Kevrekidis P G and Malomed B A 2005 *Phys. Rev. E* **71** 017602

[44] Song C S, Li J and Zong F D 2012 *Chin. Phys. B* **21** 020306

[45] Kevrekidis P G, Frantzeskakis D J and Carretero-González R 2008 *Emergent Nonlinear Phenomena in Bose-Einstein Condensates: Theory and Experiment* (New York: Springer-Verlag) Vol. 14 pp. 267–271

[46] Nistazakis H E, Kevrekidis P G, Malomed B A, Frantzeskakis D J and Bishop A R 2002 *Phys.Rev. E* **66** 015601